arXiv:physics/0008112 17 Aug 2000

DESIGN AND PERFORMANCE SIMULATIONS OF THE BUNCH COMPRESSOR FOR THE APS LEUTL FEL *

M. Borland, ANL, Argonne, IL 60439, USA

Abstract

A magnetic bunch compressor was designed and is being commissioned to provide higher peak current for the Advanced Photon Source's (APS) Low-Energy Undulator Test Line (LEUTL) free-electron laser (FEL) [1]. Of great concern is limiting emittance growth due to coherent synchrotron radiation (CSR). Tolerances must also be carefully evaluated to find stable operating conditions and ensure that the system can meet operational goals. Automated matching and tolerance simulations allowed consideration of numerous configurations, pinpointing those with reduced error sensitivity. Simulations indicate tolerable emittance growth up to 600 A peak current, for which the normalized emittance will increase from 5 to about 6.8 μm. The simulations also provide predictions of emittance variation with chicane parameters, which we hope to verify experimentally.

1 INTRODUCTION

A companion paper [2] reviews magnetic bunch compression and shows a schematic of our system. I assume the reader is familiar with this paper. The APS bunch compressor design is an outgrowth of studies [3] by P. Emma and V. Bharadwaj of Stanford Linear Accelerator Center (SLAC). They explored a number of designs, including symmetric and asymmetric four-dipole chicanes. Starting from this work, I investigated a large number of configurations with various values of R_{56}, asymmetry, and final current. For each configuration, detailed longitudinal and transverse matching was performed, followed by tracking with CSR and wakefields. Then, sensitivity analysis was performed for all configurations, followed by jitter simulations for the least sensitive configurations.

This work relied on `elegant` [4], a 6-D code with a fast simulation of CSR effects, plus longitudinal and transverse wakefields. `elegant` also performs optimization of actual tracking results, such as bunch length, energy spread, and emittance.

Simulation of the linac uses the `RFCA` element, a matrix-based rf cavity element with exact phase dependence. Our linac has quadrupoles around the accelerating structures. Hence, I split each 3-m section into about 20 pieces, between which are inserted thin-lens, 2nd-order quadrupole elements. A series of such elements is used for each quadrupole.

A Green's function technique is used to model wakefields, using a tabulation of the SLAC-structure wake functions provided by P. Emma [5]. To reduce running time, one longitudinal wake element is used per 3-m section, which is a good approximation for relativistic particles. For transverse wakes, I used one wake element per rf cavity element (about 20 per section).

The CSR model used by `elegant` is based on an equation [6] for the energy change of an arbitrary line charge distribution as a function of the position in the bunch and in a bending magnet. Details of this model will be presented by the author at an upcoming conference. Effects of changes in the longitudinal distribution within a dipole are included. CSR in drift spaces is included by propagating the terminal CSR "wake" in each bend through the drifts with the beam.

2 MATCHING

Longitudinal and transverse matching has the goal of providing configurations for the 300-A and 600-A LEUTL operating points [2]. The starting point for the simulations is macro particle data generated [7] with PARMELA, giving the 6-D distribution after the photoinjector (PI). See Figure 1 in [2].

Longitudinal matching involves adjusting the phase and voltage of L2 (see [2] for nomenclature) to obtain the desired current and energy after the chicane. Then, L4 and L5 are adjusted to minimize the energy spread and obtain the desired final energy. Longitudinal matching includes longitudinal wakefields, rf curvature, and higher-order effects in the beam transport, by matching *tracked* properties of the simulated beam.

Figure 1 shows the longitudinal phase space for the 300-A case with $R_{56} = -65$ mm, which exhibits a current spike of nearly 1200 A. The matching ignores this spike (which is shorter than a slippage length for 530 nm) because of the way "current" is defined [2].

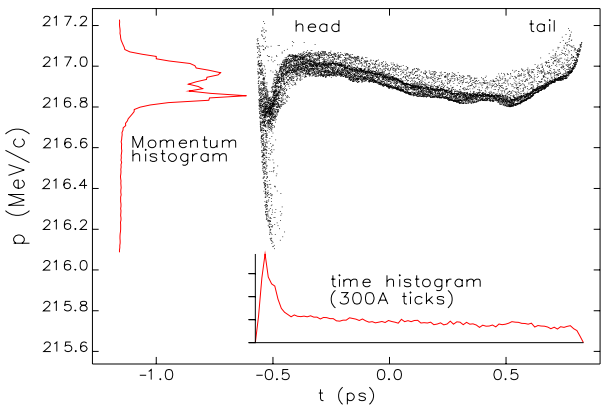

Figure 1: Typical longitudinal phase space (300-A case)

* Work supported by the U.S. Department of Energy, Office of Basic Energy Sciences, under Contract No. W-31-109-ENG-38.

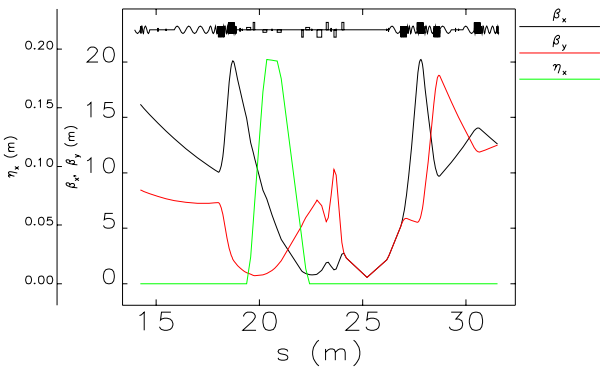

Figure 2: Typical twiss parameters in the chicane region.

Following longitudinal matching, transverse matching is done for each configuration. Initial Twiss parameters are obtained from the rms properties of the PARMELA beam. Starting values for the quadrupoles were obtained from matching "by hand" for one configuration. Four sequential `elegant` runs work the beta functions down the linac. The most important constraints maintain small beta functions in the linac (for transverse wakefield control), small horizontal beta in dipole B4 (to reduce CSR effects), and matching for the emittance measurement sections. Figure 2 shows sample Twiss parameters in the chicane region.

The matching is highly automated, so that only the desired beam current and energy needs to be specified. Evaluation of tolerances and randomized simulations are also automated, being set up by scripts from the corresponding matching runs. Transfer of data between simulation stages is handled using SDDS files and scripts [8], reducing errors and increasing the number of configurations that can be examined. For example, a script is used to scan all configurations and give power supply specifications. A distributed queue utilizing 50 workstations is used to run the simulations.

Figure 3 shows emittance vs. R_{56} for the symmetric (A=1) and asymmetric (A=2) cases at 300 A and 600 A. For 300 A, the symmetric and asymmetric cases are very similar. For 600 A, the difference is 10% or more, which should be measurable.

One surprise in Figure 3 is that the emittance does not uniformly increase as $|R_{56}|$ increases, even though `elegant` shows the expected monotonic increase (due to CSR) vs bending angle for a single dipole with a constant input beam distribution. This is apparently due to variation in the compressed bunch distribution between cases with the same "current" but different R_{56}. For smaller $|R_{56}|$, there are higher current spikes at the head of the bunch, leading to a larger and more rapidly changing CSR wake, which in turn leads to larger emittance growth. The effect is even more pronounced in the 1200-A cases (not shown). Insertion of the scraper between B2 and B3 to remove the low-energy part of the beam can reduce the height and width of the current spike, resulting in lower emittance. Unfortunately, this also reduces the current in the rest of the bunch considerably.

Earlier simulations showed that emittance trends can be changed significantly by inconsistent values of the horizontal beta function at the exit of B4. All of these subtleties will make for difficult interpretation of experiments in which R_{56} is varied. However, because compression to different currents for fixed R_{56} involves only adjustment of the rf phases and voltages, comparision of the emittance growth for different amounts of compression should be more straightforward.

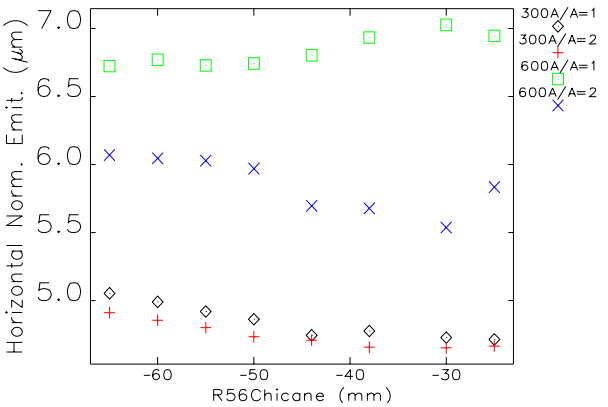

Figure 3: Horizontal normalized emittance vs. R_{56}.

3 TOLERANCE DETERMINATION

Tolerances are driven by the FEL gain length, trajectory, and wavelength stability requirements [9]. The 10% rms gain length variation limit is easy to use in `elegant` as it computes FEL performance directly using Xie's parameterization [10]. Beam trajectory limits ($\sim$50 μm, $\sim$50μr) are included separately as they are not incorporated into Xie's formula. The 1-nm rms wavelength variation limit is a challenging goal at 530 nm as it puts a 0.1% limit on energy variation.

The analysis begins by running single-parameter "sweeps" to assess the effect on the constrained quantities (gain length, trajectory, and wavelength) of accelerator parameters (e.g., rf phase). Sweeps included rf phase and voltage; photoinjector timing, charge, and energy; and chicane dipole strength. From these sweeps, a script determines the limit on each parameter change due to the various specifications, showing that configurations with the largest R_{56} are least sensitive to difficult-to-control timing and phase errors. These configurations experience the most emittance degradation from CSR, but tend to yield the shortest gain length as they have the smallest energy spread (L2 being closer to crest).

The limits, shown in Table 1, are larger for the 600-A case because the 1-nm wavelength constraint is easier at 120 nm than 530 nm. Nine parameters are limited primarily by the wavelength constraint and four others by horizontal trajectory constraints. Hence, to determine the rms tolerance, one simply divides each sweep limit by $\sqrt{N}$, N

Table 1: Selected sweep limits for $R_{56} = -65$ mm

quantity	300-A limit	600-A limit
L2 phase	0.17°	0.49°
L4/L5 phase	0.77°	1.45°
L2 voltage	0.11%	0.31%
L4/L5 voltage	0.52%	1.4%
PI timing	0.29 ps	0.88 ps
PI energy	0.26%	1.1%
PI charge	12%	>20%

being the number of parameters limited by a particular constraint. For the horizontal trajectory, N was doubled to eight to allocate half the budget to nonswept parameters (e.g., corrector magnets). Some of these phase and timing tolerances are beyond the state of the art.

4 RANDOMIZED SIMULATIONS

Randomized simulations were used to confirm the tolerances and examine errors not covered by the sweeps (e.g., corrector jitter, quadrupole jitter, and alignment). These were done for the most stable configurations (i.e., $R_{56} = -65$ mm). Because some tolerances are beyond the state of the art, I used randomized simulations to determine the impact of "relaxed" tolerances, assuming these rms levels [11]: 1° rf phase jitter, 0.1% rf voltage jitter, 1 ps timing jitter, 5% charge jitter, and 2% PI energy jitter.

Tables 2 and 3 show the results, respectively, for the sweep-derived tolerance levels and the relaxed levels. The sweep-derived tolerance levels result in meeting the specifications for the FEL, while the relaxed levels, not surprisingly, do not. One surprise in the relaxed case is the large jitter in the vertical plane. This results from uncorrected nonlinear dispersion in a vertical dogleg between the linac and the LEUTL, a problem which can be readily remediated using two sextupoles [5].

Table 2: Results of 300 randomized simulations with sweep-determined tolerance levels for $R_{56} = -65$ mm

	300 A		600 A	
quantity	rms jitter	% inside	rms jitter	% inside
$\langle x \rangle$ (μm)	71	83	57	91
$\langle x\prime \rangle$ (μr)	29	93	24	96
$\langle y \rangle$ (μm)	13	100	11	100
$\langle y\prime \rangle$ (μr)	19	98	17	99
L_{gain} (m)	0.01	99	0.016	100
λ (nm)	0.83	72	0.29	100

Table 3: Results of 300 randomized simulations with relaxed tolerance levels for $R_{56} = -65$ mm

	300 A		600 A	
quantity	rms jitter	% inside	rms jitter	% inside
$\langle x \rangle$ (μm)	89	72	89	81
$\langle x\prime \rangle$ (μr)	59	64	68	58
$\langle y \rangle$ (μm)	63	88	127	79
$\langle y\prime \rangle$ (μr)	138	62	245	39
L_{gain} (m)	0.048	68	3	1.3
λ (nm)	9.6	9	2.8	27

5 ACKNOWLEDGEMENTS

The technical note [3] by P. Emma and V. Bharadwaj provided a valuable starting point. I acknowledge helpful discussions and assistance from H. Friedsam, E. Lessner, J. Lewellen, S. Milton, and G. Travish. J. Lewellen provided the PI beam distribution data.

6 REFERENCES

[1] S.V. Milton et al., "Observation of Self-Amplified Spontaneous Emission and Exponential Growth at 530 nm," Phys. Rev. Lett., to be published.

[2] M. Borland et al., "A Highly Flexible Bunch Compressor for the APS LEUTL FEL," these proceedings.

[3] P. Emma, V. Bharadwaj, private communication.

[4] M. Borland, unpublished program. See www.aps.anl.gov/asd/oag/manuals/elegant_ver14.1 /elegant.html.

[5] P. Emma, private communication.

[6] E. L. Saldin et al., "On the coherent radiation of an electron bunch moving in an arc of a circle," NIM A 398 (1997) 392.

[7] J. Lewellen, private communication.

[8] M. Borland, "A Universal Postprocessing Toolkit for Accelerator Simulation and Data Analysis," Proc. 1998 ICAP Conference, Monterey, to be published.

[9] S. Milton, private communication.

[10] M. Xie, "Design Optimization for an X-Ray Free Electron Laser Driven by SLAC Linac," Proc. 1995 PAC, Dallas, May 1-5, 183.

[11] G. Travish, private communication.